HHS Public Access

Author manuscript

*J Mol Biol*. Author manuscript; available in PMC 2016 November 06.

Published in final edited form as:

*J Mol Biol*. 2015 November 6; 427(22): 3473–3490. doi:10.1016/j.jmb.2015.07.027.

# A highly coupled network of tertiary interactions in the SAM-I riboswitch and their role in regulatory tuning

**Christopher Wostenberg**[1], **Pablo Ceres**[2], **Jacob T. Polaski**, and **Robert T. Batey**[*]

Department of Chemistry and Biochemistry, 596 UCB, University of Colorado, Boulder, CO 80309-0596

## Abstract

RNA folding *in vivo* is significantly influenced by transcription, which is not necessarily recapitulated by $Mg^{2+}$-induced folding of the corresponding full length RNA *in vitro*. Riboswitches that regulate gene expression at the transcriptional level are an ideal system for investigating this aspect of RNA folding as ligand-dependent termination is obligatorily co-transcriptional, providing a clear readout of the folding outcome. The folding of representative members of the SAM-I family of riboswitches have been extensively analyzed using approaches focusing almost exclusively upon $Mg^{2+}$ and/or *S*-adenosylmethionine (SAM)-induced folding of full length transcripts of the ligand binding domain. To relate these findings to co-transcriptional regulatory activity, we have investigated a set of structure-guided mutations of conserved tertiary architectural elements of the ligand binding domain using an *in vitro* single-turnover transcriptional termination assay, complemented with phylogenetic analysis and isothermal titration calorimetry data. This analysis revealed a conserved internal loop adjacent to the SAM binding site that significantly affects ligand binding and regulatory activity. Conversely, most single point mutations throughout key conserved features in peripheral tertiary architecture supporting the SAM binding pocket have relatively little impact on riboswitch activity. Instead, a secondary structural element in the peripheral subdomain appears to be the key determinant in observed differences in regulatory properties across the SAM-I family. These data reveal a highly coupled network of tertiary interactions that promote high fidelity co-transcriptional folding of the riboswitch, but are only indirectly linked to regulatory tuning.

## Graphical Abstract

[*]Author to whom correspondence should be addressed, robert.batey@colorado.edu, Phone: 1-303-735-2159, Fax: 1-303-492-8425.

[1]Present address: Dept. of Science and Mathematics, California Northstate University College of Health Science, Sacramento, CA 95819-6076

[2]Present address: SomaLogic Inc., Boulder, CO 80301

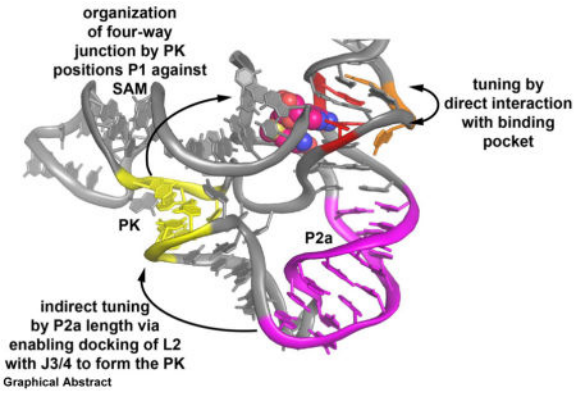

Graphical Abstract

**Keywords**

RNA structure; co-transcriptional RNA folding; S-adenosylmethionine; pseudoknot; kink-turn

## Introduction

Discoveries within the past decade have revealed that most organisms use a diverse array of noncoding RNAs to regulate important cellular functions [1–3]. Most astonishing is the mounting evidence for pervasive transcription of nearly the entire human genome with only a small minority of these transcripts known to be protein coding [4–6]. For many of these RNAs, their function is likely to be dictated by secondary and tertiary structure rather than just their primary sequence, as is the case for microRNAs and CRISPR RNAs [7]. Several decades of studying the folding of complex RNAs suggest a hierarchical model in which secondary and tertiary structure formation are decoupled [8]. Further, RNA folding is often frustrated by a rugged landscape, where misfolding leads to slow and multiphasic RNA folding [9, 10], which is problematic for short-lived and temporally constrained RNAs. The problem of misfolding becomes exponentially more challenging as the length of RNA increases, as in long non-coding RNAs which can be many kilobases in length.

However, recent studies on RNA folding are beginning to challenge these ideas. For example, tertiary interactions within the group I ribozyme are strongly coupled and cooperativity occurs early in the folding process to suppress incorrect structures [11]. The coupled and cooperative tertiary interactions assist the RNA in traversing a rugged folding landscape. Further, studies have recently started to focus on RNA structure and folding under conditions mimicking physiological conditions [12–14] or co-transcriptional constraints [15–17]. Transcriptional riboswitches are an ideal model system for studying RNA folding under co-transcriptional constraints because a regulatory decision via transcriptional termination or read-through must be made at the time the RNA polymerase reaches the poly-uridine tract of the intrinsic (rho-independent) terminator [18]. This is a relatively simple read-out of the folding outcome of the RNA during transcription. For example, a pioneering study used single molecule force extension spectroscopy to study the co-transcriptional folding of an adenine riboswitch, revealing that ligand binding inhibited transcriptional termination through formation of a temporary kinetic trap [16]. These

preliminary findings need to be extended to other riboswitches to determine if these emerging ideas are general themes.

One of the most prevalent classes of riboswitches in bacteria is the SAM clan of riboswitches (Rfam clan accession code CL00012) composed of the SAM-I (Rfam family accession code RF00162), SAM-IV (RF00634), and SAM-I/IV riboswitches (RF01725). All members of this clan bind *S*-adenosylmethionine (SAM) through a set of almost invariant sequence elements within and surrounding a central four-way junction [19–23]. The four-way junction is flanked by four helices (P1–P4; Fig. 1) that organize into two sets of coaxial stacks, P1/P4 and P2/P3, joined together by J1/2 and J3/4. The adenine nucleobase of SAM is part of a base triple with A84 and U157 (numbering based on the *Bacillus subtilis metE* SAM-I sequence, Fig. 1) within internal loop 3a (IL3a), with additional stabilization through stacking with C86. The methionine moiety makes four hydrogen bond contacts with a C83-G158•G47 base triple tying J1/2 to the P3 helix. Selectivity for SAM over its product form (*S*-adenosylhomocysteine, SAH) is due to the positively charged sulfonium group of SAM forming electrostatic interactions with the carbonyl groups of U43 and U187 (or in the case of the SAM-IV riboswitch, a guanosine) within the P1 helix.

While the binding core is almost invariant across the SAM clan, the peripheral architecture is highly divergent [20, 24–27]. The three member families of the SAM clan are distinguished by differences in their peripheral architecture around the core. The SAM-I family is defined by the presence of the PK1 subdomain (Fig. 1) and the lack of the PK2 subdomain found in the SAM-IV and SAM-I/IV families [22, 23]. The PK1 subdomain buttresses the SAM binding pocket via a characteristic pseudoknot (PK) between the hairpin loop of P2 (L2) and the J3/4 junction [28]. Positioning of L2 is promoted by a kink-turn (KT) module within P2 for SAM-I riboswitches, a feature absent in the SAM-IV family which also has the PK1 subdomain [19].

Previous studies of the SAM-I family have almost exclusively focused on conserved elements in the binding pocket and SAM binding affinity. The most important insights into the potential role of the peripheral architecture in regulatory activity have come from a study that analyzed the eleven SAM riboswitches found in the genome of *B. subtilis*. Within *B. subtilis*, the SAM-I family of riboswitches shows variations in ligand-binding affinity and switching capability both *in vitro* and *in vivo* [29]. This study found that riboswitches controlling transcriptional units regulating biosynthetic genes are responsive to lower concentrations of SAM than those regulating genes involved in transport processes. Given the absolute conservation of the core of these RNAs, these data further suggest that elements outside the binding pocket are responsible for tuning the regulatory properties of individual SAM-I riboswitches. This data is consistent with other work also showing a high degree of variation in the affinity of other SAM-I riboswitch aptamer domains for SAM [27, 30].

To define the role of tertiary interactions in the PK1 subdomain of SAM-I riboswitches in folding and regulatory activity, we chose to use the *B. subtilis metE* riboswitch (Fig. 1) as a model system. Both *in vitro* and *in vivo* experiments have shown *metE* to be a robust and functional SAM-responsive riboswitch [29]. While the aptamer of this specific riboswitch has not been characterized in depth, other binding domains from the same family with

significant sequence similarity have been studied [22, 23, 31]. The *metE* riboswitch has a high dynamic range in the context of the *in vitro* transcription assay [29, 32, 33] and the activities of the aptamer domain are modular and functional in synthetic chimeras [32, 33]. Finally, there are differences in the tertiary architecture outside the binding core compared to the other well-studied riboswitches in the SAM-I family that serve as a basis for understanding structural diversity within the SAM-I family. These include an extended P3 helix, non-canonical features within the kink-turn, and a pseudoknot composed of three base-pairs which is positioned slightly differently by having an additional base-pair in P2a. Understanding how these differences impact activity can serve to inform how variation within the family can yield regulatory tuning. Therefore, *metE* represents an ideal basis for this study because we can compare and contrast it with information gathered from other members of the SAM-I family of riboswitches.

We present *in vitro* transcription data complemented with bioinformatic and calorimetric binding analyses revealing a likely structural basis for regulatory tuning of SAM-I riboswitches. First, we demonstrate the importance of a bulged adenosine within internal loop 3b (IL3b) of P3 directly adjacent to the SAM-binding pocket. A single point deletion of this conserved adenosine is highly deleterious to function. Surprisingly, deletion or alteration of a number of conserved features throughout the PK1 subdomain have relatively little impact upon SAM-dependent transcriptional termination, with only the most severely deleterious point mutations to specific structural features showing disruption of activity. This suggests a highly cooperative network of interactions stabilizing the PK1 subdomain and its support of the SAM binding pocket. Finally, we demonstrate the loss of IL3b can be partially rescued by stabilizing mutations in the PK1 subdomain, indicating long-range coupling between this element and the peripheral architecture.

## Results

### Validation of the *B. subtilis metE* SAM-I riboswitch reporter

To assess the role of tertiary structure acquisition on riboswitch activity, we used a standard single-turnover *in vitro* transcription assay [34] to analyze a series of structure-guided mutations in the aptamer [20, 22, 23]. The single turnover *in vitro* transcription assay has been used to characterize other riboswitches including the lysine riboswitch [35, 36], the adenine riboswitch [37, 38], the magnesium riboswitch [39] and artificial riboswitches [32, 33]. This assay provides two important parameters: $T_{50}$, the amount of ligand required to elicit half-maximal regulatory response, and dynamic range (DR), the amplitude of response as the difference between fraction terminated at low and high ligand concentration. $T_{50}$ values are an indirect measurement of the binding affinity of the riboswitch for its ligand, with higher $T_{50}$ values indicating weaker binding. The dynamic range reports on the ability of the riboswitch to shift from the “ON” state to the “OFF” state under the co-transcriptional conditions, so a decrease in the dynamic range indicates a smaller population of riboswitches capable of effectively switching conformations. It is important to note in this study we used *E. coli* RNA polymerase (RNAP) rather than *B. subtilis* RNAP. While *E. coli* RNAP is less responsive to polymerase terminators [40], only minor differences in $T_{50}$s and

dynamic range have been observed between the two RNAPs for several different riboswitches [37, 41].

To validate that the *metE* riboswitch is functional in the single round *in vitro* transcription assay, initial experiments were performed with the full-length riboswitch (Fig. 2A and 2B, Table 1). The observed $T_{50}$ ($T_{50,obs}$) was 1.6 ± 0.4 μM with a dynamic range of 0.26 ± 0.01 (ranging from 0.66 to 0.92 ) (Table 1). This is a reduction in activity of the riboswitch as compared to that previously observed (dynamic range of 0.77 and a $T_{50,obs}$ of 0.5 μM) [29]. This discrepancy is likely due to variations in the methodology; notably, the prior study used a *glyQS* promoter region, pausing of the transcription reaction after initiation and stable complex formation (20–30 nucleotides), an RNA that was shorter on the 5′ end, higher magnesium concentration (10 mM versus 2.5 mM) and *B. subtilis* RNAP [24, 29]. To test if we could get an increased dynamic range consistent with previous work, we removed the first sixteen nucleotides, which we refer to as the *metE*Δ 16 variant (Fig. 1). This riboswitch has the same $T_{50,obs}$ (1.9 ± 0.5 μM) as wild type, but a significantly increased dynamic range of 0.66 ± 0.03 (ranging from 0.21 to 0.87) (Fig. 2A and 2B, Table 1). The larger dynamic range of the *metE*Δ 16 variant facilitated quantifying SAM-dependent transcriptional termination, and therefore all further experiments were performed in the context of the *metE*Δ 16 deletion.

To verify that the observed termination is the result of SAM binding, a mutation that impairs binding (U157A) was tested. This residue directly interacts with the adenine moiety of SAM [22, 23] and is universally conserved across phylogeny [42]. The U157A mutant in the context of the aptamer domain alone (spanning nucleotides 37–192: Fig. 1) weakly binds SAM with a $K_{D,obs}$ = 24 ± 7 μM as measured by isothermal titration calorimetry (ITC), whereas the wild-type aptamer domain binds with a $K_{D,obs}$ = 0.079 ± 0.008 μM (Table 2, raw thermogram data shown in Fig. S1). *N*-methylisatoic anhydride (NMIA) chemical probing (typically referred to as selective 2′-hydroxyl acylation analyzed by primer extension or "SHAPE" [43]) of the aptamer domains of the wild type riboswitch and the U157A mutant had similar nucleotide reactivity patterns without ligand (Fig. 2C), demonstrating that the U157A mutant RNA has the same local and global structure as the wild type riboswitch, analogous to a point mutation in the SAM-I/IV riboswitch [20]. Despite the same secondary and tertiary structure as wild type, the U157A abrogates all SAM-dependent NMIA chemical protection patterns observed in the wild type RNA, demonstrating that this mutant solely affects SAM binding and not RNA structure (Fig. 2D). Consistent with the above observations, the U157A mutation is incapable of promoting transcriptional termination in the presence of SAM (Table 1), demonstrating the switching observed in the *metE* riboswitch is directly due to the binding of SAM with the RNA. Most importantly, the NMIA chemical protections patterns of the *metE* aptamer domain in the presence and absence of SAM are fully consistent with those of the *B. subtilis yitJ* and *Thermoanaerobacter tengcongensis metF-H2* SAM-I aptamer domains, whose crystal structures are known [23, 28], indicating that *metE* indeed has the same structure.

### An internal loop adjacent to the SAM-binding pocket promotes ligand binding

IL3b, an internal loop within the P3 helix, has been significantly overlooked in respect to its contribution to ligand recognition by the SAM clan of riboswitches. This internal loop, which is positioned near IL3a is variable in both length and sequence, as reflected in the two crystal structures. The *T. tengcongensis metF-H2* SAM-I riboswitch aptamer crystal structure (PDB: 2GIS) has a reduced P3 helix that eliminates IL3b, a truncation made to facilitate crystallization [22]. The *B. subtilis yitJ* SAM-I riboswitch aptamer crystal structure (PDB: 4KQY) also has a reduced P3 helix, but retains IL3b [23]. In the *yitJ* crystal structure, an adenine (equivalent to A153 in *metE*) within IL3b interacts with an adenine from IL3a (equivalent to A85 in *metE*) (Fig. 3A). In this interaction, the exocyclic amino group from each adenine hydrogen bonds with the 2′ hydroxyl group of the other adenine along with π stacking of the two bases. A highly similar interaction is also observed in the crystal structure of the SAM I/IV riboswitch (PDB accession code 4OQU), albeit the composition of IL3b is slightly different [20].

We hypothesized that this interaction may be important for stabilizing the bound state of the SAM-I family of riboswitches and as such the adenine on the 3′-side of IL3b (corresponding to A153 in *metE*) will be conserved. To verify this, we used a bioinformatics approach with a subset of the sequences in the SAM-I family from Rfam 12.0 database [44]. It is important to emphasize that IL3a and the flanking Watson-Crick C-G base pairs are almost completely invariant across phylogeny, consistent with structural analyses identifying the primary site of RNA-SAM interaction. The only variation is at position 85 (numbering based on *metE* sequence): adenine is found at this position in 95.9% of sequences and guanine in 4.1%. Within IL3b, greater variation is observed with respect to both the composition and size of the loop (Fig. 3B). Of the aligned sequences, only 2.1% of them do not have IL3b, while another 5.9% do not contain an adenine corresponding to A153 in *metE* that could interact with IL3a. Thus, while an interaction between IL3a and IL3b is not a universal feature of SAM-I riboswitches, it is highly conserved and hence likely to be important for RNA function.

To address this hypothesis experimentally, we introduced a series of mutations within IL3b of the *metE* riboswitch interrogating its effect upon SAM binding. Abrogation of this element entirely by capping the P3 helix three base pairs above IL3a with a stable GAAA tetraloop (P3S, Fig. 3C) yielded an RNA displaying no detectable SAM-dependent transcriptional termination (Fig. 3C). This clearly demonstrates the essentiality of IL3b, at least in the context of the *metE* riboswitch. However, a more conservative truncation of P3 two base pairs above IL3b, again capped with a GAAA tetraloop (P3M, Fig. 3C), results in an RNA whose activity is similar to the parental *metE*Δ16 RNA with a $T_{50,obs}$ = 2.8 ± 0.6 μM and a dynamic range of 0.56 ± 0.03 (Fig. 3C, Table 1). This indicates that IL3b significantly influences riboswitch activity with minor contributions at best from sequences in P3 further distal from the binding pocket. This is consistent with the observation that beyond IL3b the sequence and structure of P3 is highly variable with no apparent conservation patterns.

The above deletion mutations only illustrate that IL3b affects riboswitch function, but do not identify specific features of the internal loop contributing to activity. To confirm that A153 is the critical residue, we tested the activity of a series of mutations that alter the size and/or composition of IL3b. Deletion of IL3b by mutating adenine 89 to guanine to form a Watson-Crick G-C pair with cytosine 152 and deleting adenine 153 (A89G/Δ153, Fig. 3D) increased the concentration of SAM required to elicit half-maximal regulatory activity by almost 50-fold ($T_{50,obs}$ = 90 ± 40 μM) as well as a diminished dynamic range to 0.24 ± 0.04 (Fig. 3D, Table 1). The A89G/Δ153 variant binds SAM very weakly ($K_{D,obs}$ = 16 ± 1 μM, Table 2), similar to the U157A variant, confirming that the reduction in riboswitch activity is due to diminished ligand binding. Deletion of A153 (Δ153, Fig. 3D) yields an RNA with similar $T_{50,obs}$ and dynamic range values as deletion of IL3b (A89G/Δ153) entirely ($T_{50}$ = 60 ± 60 μM and a dynamic range of 0.16 ± 0.05; Fig. 3D, Table 1). Furthermore, the Δ153 mutant does not bind SAM as measured by ITC (Table 2). Changing IL3b from a 1x2 internal loop to a single bulged adenine by mutating A89 to a guanine (A89G) yields an RNA with a $T_{50,obs}$ comparable to Δ16 ($T_{50,obs}$ = 2.0 ± 0.7 μM; Fig. 3D, Table 1). The ITC data supports this observation, as the $K_{D,obs}$ is only ~4-fold weaker, but the n-value (reflecting the fraction of active RNA) dropped to below 0.5 (Table 2). To determine whether the interaction between the two internal loops requires an adenine at position 153, two more point mutations were made, A153C and A153G. The increase in $T_{50,obs}$ was only minor less than five-fold indicative that an adenine at this position is preferred, but other nucleotides are tolerated (Fig. 3D, Table 1). Similarly, the binding affinity decreases by about two-fold along with a decrease in the n-value (Table 2) for both mutations, demonstrating that binding is mildly affected by these mutations. These data support the phylogenetic variability of the loop size of IL3b and the preference for an adenine at the 3′-position on the 3′-side of the loop.

## Only a consensus kink-turn in the PK1 subdomain is required for promoting ligand binding

Within the SAM clan of riboswitches (SAM-I, SAM-IV and SAM-I/IV), only the SAM-I family uses a conserved classical kink-turn module within “PK1” subdomain to position P2 adjacent to J3/J4 in order to form the pseudoknot that encapsulates the SAM binding pocket [20], and is essential for SAM binding [31]. As such, the SAM-I riboswitch aptamer has become a model system for studying the kink-turn module, providing biophysical data on its folding and structure [45–47]. However, these studies do not provide insights into how variation in the kink-turn module may affect the kinetics of folding or regulatory switching under co-transcriptional conditions. Therefore, we have assessed a series of mutants that investigate the role this module has on riboswitch function.

The importance of the kink turn module in SAM-I function is underscored by a mutation disrupting the most conserved nucleotide in the module. This single point mutant, A57C (Fig. 4), has been shown to have the strongest negative effect on the folding of the kink turn and serves as a negative control to observe the maximum effect its disruption has on riboswitch function. This adenine, along with adenine 73, participate in A-minor interactions stabilizing isolated kink-turns [48]. In the context of the *B. subtilis yitJ* SAM-I riboswitch aptamer , the mutation of the analogous adenine to a cytosine decreases $K_{D,app}$ for SAM by

almost nine-fold [31]. As expected, the A57C mutation causes loss of SAM-dependent switching from the "ON" to the "OFF" state based on our *in vitro* transcription assay (Fig. 4, Table 1) and SAM binding (Table 2). A similar mutation of adenine 73 to a cytosine (A73C) caused the dynamic range to decrease, but did not affect the $T_{50}$ (Fig. 4, Table 1), suggesting the folding of the riboswitch is modified by the A73C mutation. This agrees with the hypothesis that the A•G mismatch at position 2b•2n in the kink-turn (standard nomenclature for kink-turns [49]) in the context of the SAM-I riboswitch tolerates mutations because the kink-turn is stabilized by the adjacent pseudoknot (PK1) [46]. It is important to note that even through the 2b•2n position tolerates variation away from the canonical A•G in the SAM-I riboswitch, it is rarely observed (position 73 is an adenine in 99.7% of sequences and position 56 is an adenine in 95.4% of sequences).

Within the *metE* riboswitch there are a number of deviations from the preferred canonical kink-turn. On the 5′ side, the three-nucleotide bulge is capped by a G•U wobble instead of the canonical C-G base-pair (Fig. 4), as observed in both the consensus for *B. subtilis* SAM-I riboswitches [31] and consensus kink-turns [50]. A uridine at position 68 occurs in 3.35% of known sequences, with the more canonical C-G base pair observed more than 95%. This suggests the stronger C-G base pair is preferred to help stabilize the kink-turn structure. Unexpectedly, the U68C mutation is able to regulate transcription as well as the parental *metE*Δ16 RNA (Table 1), indicating that a wobble is well tolerated at this position.

In the canonical kink-turn, the strict consensus sequence for the bulge is RNN, with R representing a purine [50], although for SAM-I riboswitches there is a weaker consensus. Therefore, we hypothesized that the sequence of bulged nucleotides is not critical for proper function in the context of the SAM-I riboswitch. In our phylogenetic analysis the predominant sequence is GAU at 23.2%, which is observed in the *T. tengcongensis metF-H2* SAM-I riboswitch aptamer domain crystal structure [22]. The UUU bulge observed in *metE* occurs with 7% frequency, making it also a fairly common variant for the bulge. Based on the bioinformatics data, we chose to make three variants of the bulge; the most abundant variant, GAU, a variant that is observed in ~6% of sequences, AAU, and a rarely observed variant (appears less than 1% of the time in phylogeny), GUA. All these variants have relatively the same $T_{50}$ and dynamic range (Table 1), indicative that in the context of the *metE* riboswitch the bulge composition of the kink-turn has a minimal influence upon riboswitch function.

Finally, we investigated the 3b•3n position of *metE*, which is a C•C mismatch that deviates from the canonical A•G mismatch or the A•A mismatch observed in *yitJ*. Based on recent data, mismatches at this position are beneficial for metal-ion induced folding, which is expected to be important for SAM-I aptamer folding as well [47]. It must be noted that these experiments were performed with isolated duplex kink-turn containing RNAs and not in the context of SAM-I [47]. To test this observation in the context of SAM-I, we made mutations to *metE* at these positions (C55G, C74G, C74U, and C55G/C74A) and tested their ability to regulate transcription (Fig. 4, Table 1). All these mutations reduce the dynamic range with the most significant drop in dynamic range coming from C74U (Fig. 4A, Table 1), which was a decrease of 30% from $metE\Delta^{16}$, the same as the A73C variant. The change in $T_{50,obs}$ was only two-fold at most (Fig. 4A, Table 1), suggesting the binding ability is not affected

by these mutations. Instead, the folding properties of the RNA were impacted such that a reduced fraction of the population could productively terminate transcription in response to SAM.

## A minimal pseudoknot in the PK1 subdomain is required for activity

The defining feature of the PK1 subdomain in the SAM-I and SAM-IV riboswitches is a pseudoknot formed between the terminal loop of P2 (L2) and four bases in J3/4 (Fig. 1A). In the bound state, the pseudoknot is stabilized and encapsulates SAM, making it a crucial tertiary interaction in SAM-I riboswitches [28]. In the context of *yitJ*, mutations to this pseudoknot decrease binding affinity [31] and termination in both *in vitro* and *in vivo* experiments [51]. We hypothesized variation in this pseudoknot can be used to modulate the regulatory response.

Similar to the kink-turn, we created a negative control mutant to observe the maximum effect disrupting the pseudoknot will have on riboswitch function. As our negative control, we chose the G64C/G65C double mutant because an analogous mutation in *yitJ* was shown to have a ten-fold decrease on binding affinity [31]. This mutation has an even more severe effect in *metE*, as it is unable to function in the context of the *in vitro* transcription assay (Table 1) and SAM binding was not detectable by ITC (Table 2), reinforcing the importance of the pseudoknot.

The length of the P2 helix is likely to be important for precise positioning of L2 adjacent to J3/4 in order to form the pseudoknot it is expected that the riboswitch does not tolerate significant length variation in the P2 helix. Bioinformatic analysis of sequence variations in P2 shows P2b is universally three base pairs in length while there is some variation in the length of the P2a helix (Fig. 5A). The preferred length is eight Watson-Crick base pairs without any bulged/unpaired nucleotides (70.1%), while a length of nine base pairs, as observed in *metE*, is rare (1.03%). Overall, the length only varies between six and nine base pairs with generally a one or two nucleotide bulge, most often following the first Watson-Crick base pair (Fig. 5A). This indicates that the length of P2a is important for correctly positioning L2 to form the pseudoknot with J3/4. To validate this observation experimentally, four length variants of P2a were constructed from six base pairs (P2Δ 3bp) to ten base pairs (P2+1bp) (Fig. 5B, Table 1). The six, seven, and ten base pair P2a variants do not display SAM-dependent activity (Fig. 5B, Table 1). In contrast, eight and nine base pairs (P2Δ 1bp and $\Delta^{16}$) have roughly the same $T_{50}$,obs and dynamic range (Fig. 5B, Table 1). Measurements of SAM binding by ITC of these variants reveal a similar trend (Table 2). These data demonstrate that P2a is weakly tolerant of length variation, with only eight or nine base pairs supporting function.

Along with the length of P2, the ability of the pseudoknot to stably form is also predicated upon the composition of the interaction between P2 and J3/4. In *yitJ*, the pseudoknot comprises four consecutive Watson-Crick base pairs, while in the *T. tengcongensis metF-H2* SAM-I riboswitch aptamer domain there is an internal uracil-uracil mismatch that does not impair its ability to productively bind SAM.[22, 52] A uracil-uracil mismatch is also observed in *metE* (Fig. 1A), but the mismatch is at the 5′-end, creating a three Watson-Crick base pair pseudoknot. Both the three and four base pair variations of the pseudoknot are well

represented in SAM-I alignment data, with the four base pair pseudoknot being the predominant one (Fig. 5C).

To investigate the Watson-Crick base pairing requirements for this pseudoknot with respect to regulatory activity, a set of mutations were introduced into this region of the *metE* riboswitch. Mutation of U62 to adenine (U62A, Fig. 5D) to create a variant with four Watson-Crick base pairs does not affect activity (Fig. 5D, Table 1). Furthermore, placing a stronger G-C base pair (U62C/U168G, Fig. 5D) at this position as seen in *yitJ* also did not affect activity (Fig. 5D, Table 1). These data indicate that a U•U mismatch at this position of the pseudoknot is not destabilizing to the aptamer domain's architecture; this is likely true for the U•U internal mismatch as observed in the *T. tengcongensis* SAM-I riboswitch aptamer domain. Three mutations (U63A, G64C, and G65C) were made that reduce the number of Watson-Crick base pairs from three to two. In the case of the G65C mutation, the riboswitch displays no transcriptional termination activity, but the other two mutations only decrease the dynamic range without affecting the $T_{50,obs}$ (Fig. 5D, Table 1). Furthermore, if only the G65-C165 base pair is present (U63A/G64C), the riboswitch is unable to function (Fig. 5D, Table 1). Therefore, the pseudoknot must be composed of at least two base pairs with one of them being the G65-C165 base-pair.

The other highly conserved tertiary interaction element in the PK1 subdomain that aids in stabilizing the pseudoknot are two adenosines in J3/4 that form minor groove triples with G-C pairs in P2b (A161•G59-C67 and A162•G60-C66) and a third triple between A61 of L2 and the U164-A184 pair. Based on our data for base pairing of the pseudoknot, we expect mutations disrupting the base triples would have modest effect on *metE* riboswitch function. The nucleotides involved in the base triples within J3/4 were each mutated to cytosine (A161C, A162C, U164C; Fig. 5E). In the case of U164C, the mutant is able to regulate transcription as well as the parental *metE*Δ 16 RNA with respect to both dynamic range or the $T_{50,obs}$ (Fig. 5E, Table 1). We saw similar results with A61C (Table 1), together, these data indicates the U164-A184•A61 triple is at most weakly stabilizing the pseudoknot. In contrast, both A161C and A162C decrease the $T_{50,obs}$ (seven-fold and two-fold, respectively; Figure 5E, Table 1), illustrating their importance in stabilizing the pseudoknot and thus the bound state. This agrees with our mutagenesis data from the base pairing of the pseudoknot where mutations affecting G65-C165 base pair are more detrimental than mutations affecting the U62•U168 mismatch. Interestingly, a double mutant (A161C/A162C, Fig. 5E) of these residues was able to restore wild-type parameters. One explanation for this is that two pyrimidines or two purines can both productively interact with the minor groove whereas in a one pyrimidine/one purine combination the purine pushes the pyrimidine residue away from the groove.

## Coupling of IL3b and the PK1 subdomain

Above, we have shown that only a few point mutations within the peripheral elements of the *metE* aptamer have a significant effect on riboswitch function. Generally, there is one nucleotide or base pair within each element that is critical for regulatory activity: A153 in IL3b, A57•G72 in the kink turn, G65-C165 in the pseudoknot and A161 in the J3/4-P2b base-triples. Most other mutations tested had only minor impacts upon activity. One of the

most unexpected results from this was that deletion of IL3b completely abolished SAM binding and regulation in the *metE* riboswitch, as a number of natural SAM-I aptamers lack this element. Furthermore, we have extensively studied a variant of the *T. tengcongensis metF-H2* SAM-I riboswitch aptamer domain that has the IL3b removed and the riboswitch can still effectively bind SAM and switch from the "ON" state to the "OFF" state.[22, 52, 53]

To validate that in the context of the *T. tengcongensis metF-H2* riboswitch, deletion of IL3b is tolerated; we tested SAM binding by wild type and an IL3b deletion mutant (*metF-H2*(Δ60)) by ITC. The *metF-H2* wild type aptamer has a similar affinity for SAM as *metE* ($K_D$ = 0.07 ± 0.01 μM for *metF-H2* compared to $K_D$ = 0.079 ± 0.008 μM for *metE*, Table 2). However, *metF-H2* Δ60 has less than a 10-fold reduction in SAM binding affinity, whereas *metE*Δ 153 shows very weak binding (Table 2). This illustrates that deletion of the bulged adenine in IL3b abolishes activity only in a subset of SAM-I riboswitches.

This observation led us to hypothesize that the loss of IL3b can be compensated for by potentially more energetically favorable tertiary interactions in the PK1 subdomain. To validate this, we designed two double mutants of the nonfunctional *metE*(Δ153) variant. The first double mutant strengthened the pseudoknot by converting the U•U mismatch to an A-U base pair (U62A/Δ153). The other double mutant shortened the P2a helix by a base pair in order to better position the L2 and the J3/J4 junction for pseudoknot formation (P2Δ1/Δ153). Both mutations are distal to the original Δ153 mutation (Fig. 1), and thus any effect they have on the riboswitch should be due to overall folding cooperativity and not direct communication. These single mutations were chosen because each has no major effect on riboswitch function in the context of the wild type IL3b (Tables 1 and 2). In both cases, measurable binding was restored to the riboswitch (Table 2) along with regulatory activity (Fig. 6A, Table 1). Therefore, in the absence of IL3b, the stability of the PK1 subdomain becomes critical for binding and activity.

## Discussion

Previous studies of the SAM-I riboswitch family have revealed that despite a nearly universally conserved set of nucleotides that directly interact with the ligand, they exhibit a marked diversity of affinities and regulatory activities [27, 29]. For the eleven SAM-I riboswitches found in *B. subtilis*, this was hypothesized to "tune" the regulatory properties of the riboswitch to the needs of the transcriptional unit [29] a feature that has been proposed in other riboswitches as well [54, 55]. Despite these clear observations, the structural or mechanistic basis for this property of SAM-I riboswitches has remained unclear. At the outset of this study, our hypothesis was that peripheral tertiary elements of the SAM-I riboswitch, particularly in the PK1 subdomain, are responsible for stabilizing and maintaining the binding affinity and functionality of the riboswitch. We explored this hypothesis by investigating tertiary structures outside the binding pocket of the *metE* riboswitch from *B. subtilis* and comparing it with the highly investigated *B. subtilis yitJ* and *T. tengcongensis metF-H2* SAM-I riboswitches.

Using an activity-based approach, this study revealed novel aspects about the role of conserved structural elements in the SAM-I riboswitch that contribute to ligand binding and transcriptional regulation. First, the importance of an interaction between IL3a and IL3b in the SAM-I riboswitch was established. Comparison of the *yitJ* and *metF-H2* SAM-I riboswitch aptamer domain crystal structures shows that the presence of IL3b does not affect the global fold of the SAM-I aptamer or the local structure of the binding pocket, including the adenine of IL3a that directly interacts with IL3b [22, 23]. Instead, NMIA chemical probing of *metF-H2* in the presence and absence of IL3b indicate that this interaction substantially reduces the dynamics of adenine 85. In the absence of IL3b, the reactivity of this nucleotide is enhanced upon SAM binding, indicating high conformational flexibility and/or structural dynamics of the local backbone, whereas in the presence of IL3b its reactivity is reduced [23, 53]. Thus, the IL3a/IL3b interaction likely facilitates SAM binding by rigidifying part of the internal loop that forms the SAM binding site upon ligand binding. Mutation of A153 to any other nucleotide only has a minor effect on the binding affinity (Table 2) and functionality of the riboswitch (Table 1). However, deletion of the adenine abrogates binding (Table 2) and regulatory activity (Table 1) in the context of the *metE* SAM-I riboswitch.

IL3b has the potential to be a means of tuning the regulatory activity of SAM-I riboswitches. This is clearly illustrated by the finding that the identity of the nucleotide at position 153 impacts regulatory activity as the A153C point substitution causes $T_{50,obs}$ to increase by at least four-fold (Table 1). These data indicate that IL3b is an element spatially close to the binding pocket that can tune the switching properties of the SAM-I riboswitch. In addition, the loss of IL3b as observed in ~2% of a subset of known SAM-I riboswitches, negatively impacts regulatory activity. An example is the *B. subtilis yoaD* riboswitch that has reduced activity both *in vitro* and *in vivo* as compared with other SAM-I riboswitches (Fig. 7A) [29]. However, the requirement for IL3b in promoting SAM binding may not be the same in all members of the SAM-I family. SAM binding by the *T. tengcongensis metF-H2* riboswitch is only moderately affected by deletion of the critical adenine of IL3b (Table 2). A number of studies on the recognition of SAM by the ΔIL3b variant of the *T. tengcongensis metF-H2* SAM-I aptamer indicates its specificity for SAM is similar to that of SAM-I aptamers with the internal loop [23, 28, 53]. Thus, there are likely other features of the SAM-I aptamer influencing the requirement of IL3b.

The role of a conserved element proximal to the ligand binding pocket in SAM-I in modulating small molecule binding is similar to what has been observed in other riboswitches, notably the purine [54] and the FMN [55] riboswitches. In the purine riboswitch aptamer, an element within P2 adjacent to the three-way junction housing the purine nucleobase binding pocket modulates binding affinity as well as regulatory activity [54]. In the FMN riboswitch, tuning of the binding affinity is dependent on the base pair composition and sequence context of the aptamer helices, with G-C base-pairs favored over A-U or G-U base-pairs for high affinity binding [55]. This property may be a general feature of RNA-small molecule interactions. For example, sequences in a Watson-Crick paired helix adjacent to the Tat binding site in the HIV transactivation response element RNA affects Tat

binding [56]. Our current findings continue to establish this as an emerging theme in RNA-small molecule interactions.

Expectedly, the conserved PK1 subdomain also has a significant effect on regulatory activity. Previous studies of a SAM-I riboswitch using binding and activity approaches revealed the importance of the kink-turn motif [31] and the P4 helix [30]. To further define the role of tertiary interactions in the PK1 subdomain on regulatory activity, we focused on its four constituent structural elements: the P2a helix, the kink-turn, the pseudoknot and the A-minor triples between J3/4 and P2b (Figure 1). Each of these elements displays sequence and structural variation within the SAM-I riboswitch family, as observed in phylogenetic sequence alignments. Surprisingly, these data revealed that only a single nucleotide or base pair within these elements are capable of completely abrogating SAM-dependent regulatory function: A153 in IL3b, A57•G72 within the kink-turn, and G65-C165 within the pseudoknot. Other than these few sites, the *metE* riboswitch is broadly tolerant of mutations even in highly phylogenetically conserved regions, such as A73, U68, A61 and U164.

In light of the above data, we propose that rather than destabilizing tertiary structural elements in PK1 to adjust ligand binding and regulatory activity, the SAM-I riboswitches use the length of the P2a helix for tuning. Our data indicate that the RNA is fairly restrictive in the lengths of this helix that are tolerated: eight or nine base pairs (as defined by the constraints of the four-way junction at the 5′-side and the three-nucleotide bulge of the kink turn on its 3′-side, as observed in crystal structures) in the context of *metE*. In the eleven *B. subtilis* SAM-I riboswitches, the variants with the strongest regulatory activity (*in vitro* $T_{50}$ < 1 μM; [29]) all have a consensus IL3b loop and eight or nine base pairs in P2b (*metI*, *metE*, *mtnK* and *yitJ*; Figure 7A). Variants with intermediate $T_{50}$s between 1 and 10 μM (*ykrW*, *yxjG* and *yxjH*) have IL3b but tend to have shorter P2a helices (seven base pairs). These helices also tend to have a single bulged adenosine following the first Watson-Crick pair that may partially support the shorter helical length. It should be noted that in the *T. tengcongensis metF-H2* crystal structure, this nucleotide was bulged out of the helix such that the first and second Watson-Crick pairs stack [22]. Finally, the variants showing the lowest regulatory activity ($T_{50}$ > 10 μM) *yoaD* and *yusC* (along with the *cysH* and *yxhH* variants that showed no activity) either lack IL3b or have short P2a helices. Notably, these variants also tend to lack the bulged adenosine between the first and second base pair of P2a. Thus, we propose that IL3b and the P2a helix are the primary tuning elements of the SAM-I riboswitches. The likely mechanism for P2a length variation is the positioning of L2 for base pairing with J3/4 to form the defining pseudoknot of the PK1 subdomain. Shorter P2a helices create either a thermodynamic or kinetic penalty for proper formation of the tertiary architecture in this region of the RNA, thereby requiring higher concentrations of SAM to effect transcriptional termination.

The observation that only the most deleterious mutations in each tertiary module significantly affect regulatory activity supports the hypothesis that the PK1 subdomain is stabilized through a highly cooperative network of tertiary interactions. This is consistent with the hypothesis that the A73C mutation in the kink-turn is not detrimental to SAM binding because the pseudoknot helps to stabilize the kink-turn in the context of the SAM-I riboswitch, but the same mutation in the context of the isolated kink-turn completely

destabilizes the motif [46]. This also explains the minimal effect the G•U wobble on the 5′ side and the mutations at position 3b•3n of the kink-turn have on riboswitch function (Table 1). Additionally, this explains the observation that only two non-contiguous Watson-Crick base pairs in the pseudoknot are required for function, a situation that would be expected to be highly destabilizing.

Further, IL3b and the PK1 subdomain are coupled with respect to their ability to promote SAM binding and regulatory activity. As demonstrated by the *T. tengcongensis metF-H2* riboswitch aptamer, the presence of IL3b is not essential for SAM binding. This is likely because the PK1 subdomain contains the optimal set of tertiary interactions that can support ligand binding. In contrast, *metE* regulatory function is greatly weakened when IL3b is deleted. Regulatory function of *metE* in the context of the ΔIL3b mutation can be by partially restored by optimizing the PK1 subdomain either through repositioning (P2Δ1/Δ153) or strengthening (U62A/Δ153) the pseudoknot. Thus, the PK1 subdomain and IL3b are coupled in support of binding of SAM to the core (Fig. 7B).

In addition to reducing the effect point mutations have on riboswitch function, the coupled network potentially organizes the aptamer for efficient ligand binding. It has already been demonstrated that the pseudoknot stabilizes the bound state while encapsulating the SAM ligand [28]. In this study, we showed that the bulged adenine in IL3b interacts with an adenine in IL3a in the major groove away from the binding pocket, which promotes SAM binding. Interestingly, A85 in the unbound *T. tengcongensis* (ΔIL3b)SAM-I riboswitch occupies the SAM binding pocket by forming a triple with A84 and U157 [53]. Thus, another purpose of A153 might be to promote the “open” state of the SAM binding pocket for direct interaction of the adenosine moiety of the ligand. It has already been hypothesized that the role of the auxiliary elements, specifically the P4 helix, in the SAM-I riboswitch is to optimize ligand affinity by organizing the aptamer [30]. Like our point mutations, removal of the P4 helix causes only a minor increase in the $T_{50,obs}$, indicative of it having an indirect contribution to riboswitch binding and function. Organization of the binding pocket for efficient ligand binding by peripheral tertiary architectural elements is a common feature of riboswitch aptamer domains [57, 58].

The coupling of the tertiary interactions within PK1 subdomain and P3 is critical for co-transcriptional folding, as these structures are transcribed early, and thus have a greater impact on proper folding of the SAM-I riboswitch aptamer domain [17]. It has been shown computationally and experimentally that RNA structures fold in the order in which they are transcribed, and that competing structures can invade the previous structure if they further stabilize the RNA [16, 17]. Therefore, strengthening of tertiary elements that form early in transcription through a coupling network helps to promote the proper RNA fold while discouraging misfolding. This is reflected in our data where point mutations that weaken tertiary elements affect the folding as illustrated by the decrease in the dynamic range without impacting binding ability (Table 1). Coupled tertiary interactions that form early in the folding process have been observed in the group I self-splicing intron, which promote proper RNA folding by suppressing nonnative structures [11]. The network of peripheral tertiary elements might be more important within the cellular environment as RNA tertiary interactions are strengthened relative to secondary interactions within macromolecular

crowders and cosolutes [12]. The highly coupled nature of tertiary structure in RNA also likely makes it poorly suited for modulation of activity such as regulatory tuning. Rather, secondary structure is more ideal as minor changes to the length of a helix or introduction of distortions to the helix that only require one or several point substitutions or an insertion/deletion can affect an entire set of tertiary interactions. Thus, we propose that secondary rather than tertiary structure has a more significant affect on variation in RNA activity between orthologs.

In conclusion, these findings continue to build a picture of RNA folding and function under co-transcriptional constraints. Specifically for riboswitches, peripheral tertiary elements are key for ligand dependent RNA switching during transcription. In general, a network of highly coupled tertiary interactions likely serves to promote native structure folding early in transcription while suppressing nonnative structures. This view of co-transcriptional folding is clearly reflected in single molecule observations of an adenine-responsive riboswitch [16]. The coupled nature of these tertiary interactions, however, makes secondary structure the more appropriate structural elements for activity tuning in RNA through the ability of small changes at this level of structure to globally affect a network of tertiary interactions. Further work still needs to be done to translate these ideas into RNA folding and activity in the cellular environment where the presence of proteins and various cosolutes will certainly impact these processes in ways that may not be reflected in approaches such as the minimal assay used in this study. Nonetheless, these results are part of the important first steps in addressing this aspect of RNA folding and function in the co-transcriptional context.

## Materials and Methods

### Construction of DNA vectors

DNA vectors were synthesized by either recursive PCR or site-directed mutagenesis [59] from DNA oligonucleotides (Integrated DNA Technologies). In both cases, *Pfu* DNA polymerase was used with standard reaction buffer conditions. For site-directed mutagenesis, DMSO was added to a final concentration of 1% to prevent primer dimers and denature any inherent structure in the template. For vectors encoding genes used for single-turnover transcription assays, the T7A1 bacterial RNA polymerase promoter (5′TTATCAAAAAGAGTA- TTGACTTAAAGTCTAACCTATAGGATACTTACAGCC) was placed immediately upstream of the transcription start site for each riboswitch construct. The sequences were cloned into pUC19 (New England Biolabs) via the EcoRI and HindIII restriction digest sites within the multiple cloning site. Sequences were verified prior to use in transcription assays; complete sequences of all constructs are given in supplementary information Table S1.

### Single-turnover *in vitro* transcription assays

Single-turnover transcriptions were performed as previously described [39, 60]. In brief, transcription templates were PCR amplified from sequence-verified vectors with *Pfu* DNA polymerase. The DNA was purified using a Qiagen PCR clean-up kit. 50 to 100 ng of template DNA was incubated at 37 °C for 15 minutes in *E. coli* RNA polymerase (RNAP) transcription buffer (70 mM TrisCl, pH 8.0, 70 mM NaCl, 0.1 mM EDTA, 14 mM β-

mercaptoethanol, and 35 μg/mL BSA), 2.5 mM $MgCl_2$, 1 μCi of [α-$^{32}$P]ATP, and 0.25 units of *E. coli* RNA polymerase σ70 holoenzyme (Epicentre Biotechnologies) to a final volume of 17.5 μL. Addition of 7.5 μL of NTP mix (rNTPs in equal molar ratios of 165 μM), 0.2 mg/mL heparin, and the desired concentration of SAM initiated the reaction. The reactions were quenched after 15 minutes at 37 °C by adding 25 μL 8 M urea. Read-through and terminated transcription products were separated using a denaturing 6% 29:1 acrylamide:bisacrylamide gel. The gel was dried and then exposed to a phosphor screen overnight. RNA band intensities were quantified using ImageJ (http://imagej.nih.gov/ij/). The data was collected in triplicate and the average values, with the standard deviation used for weighting, were used for fitting to a standard two-state model by nonlinear least square analysis in Igor (WaveMetrics).

## Isothermal Titration Calorimetry (ITC)

The aptamer domain (nucleotides 31 to 201) of the *metE* riboswitch and the mutants thereof were PCR amplified from the pUC19 vector using the *Pfu* DNA polymerase (forward, 5′GAAATTAATACGACTCACTATAGGCATTTTCTCTTATCGAGAGTTG; reverse, 5′CAC-TGCCTCTCTCATCTCTCA). RNA was transcribed from the DNA template using T7 RNA polymerase and purified by denaturing polyacrylamide gel electrophoresis (PAGE) [61]. The purified RNA was dialyzed overnight at 4 °C in 50 mM TrisCl, pH 8.0, 135 mM KCl, 15 mM NaCl, and 10 mM $MgCl_2$. After dialysis, the buffer was filtered through a 2.0 μm membrane and used for washing the ITC cell and dissolving SAM. The exact concentrations and c-values used in the experiment are shown in supplementary information Table S2. Prior to each ITC run, the RNA was heated to 95 °C for a minute and then snap-cooled in order to refold the RNA. Two hundred seventy microliters of RNA was loaded into the cell and forty microliters of SAM was loaded into the syringe. Thirty-one injections were done for each titration; the first injection was 0.2 microliters and the rest were 1.2 microliters. The first injection was omitted from data processing. All injection durations were twice the volume in seconds and had a filter time of 5 seconds. The experiments were done on the MicroCal $iTC_{200}$ system at a temperature of 37 °C to match the transcription assays, a reference power of eleven, sixty second initial delay, 1000 rpm stirring speed and the high feedback mode. Data were analyzed using the Origin ITC software (MicroCal Software Inc.) with a single-site binding model. Examples of the thermograms are shown in supplementary information Figure S1. All the values reported represent averages from three independent experiments with error values reported as standard deviations.

## SHAPE probing

Similar to ITC experiments, the aptamer domain (nucleotides 31 to 201) of wild type and the U157A mutant (SAM binding knock-out) were synthesized using T7 RNA polymerase and purified by denaturing PAGE. Forward primer for PCR was the same as ITC and reverse primer, containing the SHAPE cassette, was 5′-GAACCGGACCGAAGCCCGATTTGGATCC-GGCGAACCGGATCGCACTGCCTCTCTCATCTCTCA. Chemical probing was performed using *N*-methylisotoic anhydride (NMIA) as previously described with slight modifications [62]. For probing reactions, 10 μL reactions were prepared to final concentrations of 100 nM RNA, 100 mM Na-HEPES, pH 8.0, 100 mM NaCl, 1 mM $MgCl_2$,

1 mM SAM, and 6.5 mM NMIA. Probing reactions were incubated at 37 °C for 41 minutes (five half-lives). Following probing, primer extension using reverse transcriptase was carried out as previously described [62]. Products were separated using 12% denaturing PAGE and visualized using a Typhoon 9400 PhosphoroImager (Molecular Dynamics). Reactivity profiles for each RNA were calculated using the SAFA software package [63].

### Bioinformatic analysis

The whole alignment for the SAM-I riboswitch family was downloaded from Rfam 12.0 [44] which contained 4757 sequences. The alignment was reduced to 388 sequences by setting 95% redundancy cut-off in Jalview [64], to obtain a workable subset that was diverse in both discrete sequences and bacterial species. The sequences were analyzed in Jalview and Emacs (http://www.gnu.org/software/emacs/) with the Ralee add-on [65]. The alignment is provided in supplementary information Table S3.

## Supplementary Material

Refer to Web version on PubMed Central for supplementary material.

## Acknowledgments

This work has been funded by a grant to R.T.B. from the National Institutes of Health (R01 GM083953) to R.T.B. and through an award by the NIH/CU Molecular Biophysics Training Program (T32 GM06103) to J.T.P.

## Abbreviations

| | |
|---|---|
| **IL** | internal loop |
| **ITC** | isothermal titration calorimetry |
| **KT** | kink-turn |
| **PK** | pseudoknot |
| **RNAP** | RNA polymerase |
| **SAM** | *S*-adenosylmethionine |
| **SAH** | *S*-adenosylhomocysteine |
| **SHAPE** | selective 2′-hydroxyl acylation analyzed by primer extension |

## References

1. Michaux C, Verneuil N, Hartke A, Giard JC. Physiological roles of small RNA molecules. Microbiology. 2014; 160:1007–19. [PubMed: 24694375]
2. Babski J, Maier LK, Heyer R, Jaschinski K, Prasse D, Jager D, et al. Small regulatory RNAs in Archaea. RNA Biol. 2014; 11:484–93. [PubMed: 24755959]
3. Batista PJ, Chang HY. Long noncoding RNAs: cellular address codes in development and disease. Cell. 2013; 152:1298–307. [PubMed: 23498938]
4. Lander ES. Initial impact of the sequencing of the human genome. Nature. 2011; 470:187–97. [PubMed: 21307931]
5. Feingold EA, Good PJ, Guyer MS, Kamholz S, Liefer L, Wetterstrand K, et al. The ENCODE (ENCyclopedia of DNA elements) Project. Science. 2004; 306:636–40. [PubMed: 15499007]

6. Birney E, Stamatoyannopoulos JA, Dutta A, Guigo R, Gingeras TR, Margulies EH, et al. Identification and analysis of functional elements in 1% of the human genome by the ENCODE pilot project. Nature. 2007; 447:799–816. [PubMed: 17571346]
7. Lagana A, Shasha D, Croce CM. Synthetic RNAs for Gene Regulation: Design Principles and Computational Tools. Front Bioeng Biotechnol. 2014; 2:65. [PubMed: 25566532]
8. Greenleaf WJ, Frieda KL, Foster DAN, Woodside MT, Block SM. Direct observation of hierarchical folding in single riboswitch aptamers. Science. 2008; 319:630–3. [PubMed: 18174398]
9. Sclavi B, Sullivan M, Chance MR, Brenowitz M, Woodson SA. RNA folding at millisecond intervals by synchrotron hydroxyl radical footprinting. Science. 1998; 279:1940–3. [PubMed: 9506944]
10. Swisher JF, Su LHJ, Brenowitz M, Anderson VE, Pyle AM. Productive folding to the native state by a group II intron ribozyme. Journal of Molecular Biology. 2002; 315:297–310. [PubMed: 11786013]
11. Behrouzi R, Roh JH, Kilburn D, Briber RM, Woodson SA. Cooperative Tertiary Interaction Network Guides RNA Folding. Cell. 2012; 149:348–57. [PubMed: 22500801]
12. Strulson CA, Boyer JA, Whitman EE, Bevilacqua PC. Molecular crowders and cosolutes promote folding cooperativity of RNA under physiological ionic conditions. Rna-a Publication of the Rna Society. 2014; 20:331–47.
13. Dupuis NF, Holmstrom ED, Nesbitt DJ. Molecular-crowding effects on single-molecule RNA folding/unfolding thermodynamics and kinetics. Proceedings of the National Academy of Sciences of the United States of America. 2014; 111:8464–9. [PubMed: 24850865]
14. Stephenson W, Keller S, Santiago R, Albrecht JE, Asare-Okai PN, Tenenbaum SA, et al. Combining temperature and force to study folding of an RNA hairpin. Physical Chemistry Chemical Physics. 2014; 16:906–17. [PubMed: 24276015]
15. Nechooshtan G, Elgrably-Weiss M, Altuvia S. Changes in transcriptional pausing modify the folding dynamics of the pH-responsive RNA element. Nucleic Acids Research. 2014; 42:622–30. [PubMed: 24078087]
16. Frieda KL, Block SM. Direct Observation of Cotranscriptional Folding in an Adenine Riboswitch. Science. 2012; 338:397–400. [PubMed: 23087247]
17. Lutz B, Faber M, Verma A, Klumpp S, Schug A. Differences between cotranscriptional and free riboswitch folding. Nucleic Acids Research. 2014; 42:2687–96. [PubMed: 24275497]
18. Roth A, Breaker RR. The Structural and Functional Diversity of Metabolite-Binding Riboswitches. Annual Review of Biochemistry. 2009:305–34.
19. Breaker RR. Riboswitches and the RNA World. Cold Spring Harbor Perspectives in Biology. 2012:4.
20. Trausch JJ, Xu ZJ, Edwards AL, Reyes FE, Ross PE, Knight R, et al. Structural basis for diversity in the SAM clan of riboswitches. Proceedings of the National Academy of Sciences of the United States of America. 2014; 111:6624–9. [PubMed: 24753586]
21. Lu CR, Smith AM, Ding F, Chowdhury A, Henkin TM, Ke AL. Variable Sequences outside the Sam-Binding Core Critically Influence the Conformational Dynamics of the SAM-III/SMK Box Riboswitch. Journal of Molecular Biology. 2011; 409:786–99. [PubMed: 21549712]
22. Montange RK, Batey RT. Structure of the S-adenosylmethionine riboswitch regulatory mRNA element. Nature. 2006; 441:1172–5. [PubMed: 16810258]
23. Lu CR, Ding F, Chowdhury A, Pradhan V, Tomsic J, Holmes WM, et al. SAM Recognition and Conformational Switching Mechanism in the Bacillus subtilis yitJ S Box/SAM-I Riboswitch. Journal of Molecular Biology. 2010; 404:803–18. [PubMed: 20951706]
24. McDaniel BAM, Grundy FJ, Artsimovitch I, Henkin TM. Transcription termination control of the S box system: Direct measurement of S-adenosylmethionine by the leader RNA. Proceedings of the National Academy of Sciences of the United States of America. 2003; 100:3083–8. [PubMed: 12626738]
25. Weinberg Z, Regulski EE, Hammond MC, Barrick JE, Yao Z, Ruzzo WL, et al. The aptamer core of SAM-IV riboswitches mimics the ligand-binding site of SAM-I riboswitches. Rna-a Publication of the Rna Society. 2008; 14:822–8.

26. Weinberg Z, Wang JX, Bogue J, Yang JY, Corbino K, Moy RH, et al. Comparative genomics reveals 104 candidate structured RNAs from bacteria, archaea, and their metagenomes. Genome Biology. 2010:11.
27. Winkler WC, Nahvi A, Sudarsan N, Barrick JE, Breaker RR. An mRNA structure that controls gene expression by binding S-adenosylmethionine. Nature Structural Biology. 2003; 10:701–7. [PubMed: 12910260]
28. Hennelly SP, Sanbonmatsu KY. Tertiary contacts control switching of the SAM-I riboswitch. Nucleic Acids Research. 2011; 39:2416–31. [PubMed: 21097777]
29. Tomsic J, McDaniel BA, Grundy FJ, Henkin TA. Natural variability in S-adenosylmethionine (SAM)-dependent riboswitches: S-box elements in Bacillus subtilis exhibit differential sensitivity to SAM in vivo and in vitro. Journal of Bacteriology. 2008; 190:823–33. [PubMed: 18039762]
30. Heppell B, Blouin S, Dussault AM, Mulhbacher J, Ennifar E, Penedo JC, et al. Molecular insights into the ligand-controlled organization of the SAM-I riboswitch. Nature Chemical Biology. 2011; 7:384–92. [PubMed: 21532599]
31. Heppell B, Lafontaine DA. Folding of the SAM aptamer is determined by the formation of a K-turn-dependent pseudoknot. Biochemistry. 2008; 47:1490–9. [PubMed: 18205390]
32. Ceres P, Trausch JJ, Batey RT. Engineering modular 'ON' RNA switches using biological components. Nucleic Acids Research. 2013; 41:10449–61. [PubMed: 23999097]
33. Ceres P, Garst AD, Marcano-Velazquez JG, Batey RT. Modularity of Select Riboswitch Expression Platforms Enables Facile Engineering of Novel Genetic Regulatory Devices. Acs Synthetic Biology. 2013; 2:463–72. [PubMed: 23654267]
34. Artsimovitch I, Henkin TM. In vitro approaches to analysis of transcription termination. Methods. 2009; 47:37–43. [PubMed: 18948199]
35. Blouin S, Lafontaine DA. A loop-loop interaction and a K-turn motif located in the lysine aptamer domain are important for the riboswitch gene regulation control. Rna-a Publication of the Rna Society. 2007; 13:1256–67.
36. Garst AD, Porter EB, Batey RT. Insights into the Regulatory Landscape of the Lysine Riboswitch. Journal of Molecular Biology. 2012; 423:17–33. [PubMed: 22771573]
37. Lemay JF, Desnoyers G, Blouin S, Heppell B, Bastet L, St-Pierre P, et al. Comparative Study between Transcriptionally- and Translationally-Acting Adenine Riboswitches Reveals Key Differences in Riboswitch Regulatory Mechanisms. Plos Genetics. 2011:7.
38. Marcano-Velazquez JG, Batey RT. Structure-guided Mutational Analysis of Gene Regulation by the Bacillus subtilis pbuE Adenine-responsive Riboswitch in a Cellular Context. The Journal of Biological Chemistry. 2015; 290:4464–75. [PubMed: 25550163]
39. Dann CE, Wakeman CA, Sieling CL, Baker SC, Irnov I, Winkler WC. Structure and mechanism of a metal-sensing regulatory RNA. Cell. 2007; 130:878–92. [PubMed: 17803910]
40. Artsimovitch I, Svetlov V, Anthony L, Burgess RR, Landick R. RNA polymerases from Bacillus subtilis and Escherichia coli differ in recognition of regulatory signals in vitro. Journal of Bacteriology. 2000; 182:6027–35. [PubMed: 11029421]
41. Wickiser JK, Winkler WC, Breaker RR, Crothers DM. The speed of RNA transcription and metabolite binding kinetics operate an FMN riboswitch. Molecular Cell. 2005; 18:49–60. [PubMed: 15808508]
42. Grundy FJ, Henkin TM. The S box regulon: a new global transcription termination control system for methionine and cysteine biosynthesis genes in Gram-positive bacteria. Molecular Microbiology. 1998; 30:737–49. [PubMed: 10094622]
43. Merino EJ, Wilkinson KA, Coughlan JL, Weeks KM. RNA structure analysis at single nucleotide resolution by selective 2 '-hydroxyl acylation and primer extension (SHAPE). Journal of the American Chemical Society. 2005; 127:4223–31. [PubMed: 15783204]
44. Gardner PP, Daub J, Tate JG, Nawrocki EP, Kolbe DL, Lindgreen S, et al. Rfam: updates to the RNA families database. Nucleic Acids Research. 2009; 37:D136–D40. [PubMed: 18953034]
45. Daldrop P, Masquida B, Lilley DMJ. The functional exchangeability of pk- and k-turns in RNA structure. Rna Biology. 2013; 10:445–52. [PubMed: 23364423]
46. Schroeder KT, Daldrop P, Lilley DMJ. RNA Tertiary Interactions in a Riboswitch Stabilize the Structure of a Kink Turn. Structure. 2011; 19:1233–40. [PubMed: 21893284]

47. McPhee SA, Huang L, Lilley DMJ. A critical base pair in k-turns that confers folding characteristics and correlates with biological function. Nature Communications. 2014:5.
48. Nissen P, Ippolito JA, Ban N, Moore PB, Steitz TA. RNA tertiary interactions in the large ribosomal subunit: The A-minor motif. Proceedings of the National Academy of Sciences of the United States of America. 2001; 98:4899–903. [PubMed: 11296253]
49. Liu J, Lilley DMJ. The role of specific 2 '-hydroxyl groups in the stabilization of the folded conformation of kink-turn RNA. Rna-a Publication of the Rna Society. 2007; 13:200–10.
50. Klein DJ, Schmeing TM, Moore PB, Steitz TA. The kink-turn: a new RNA secondary structure motif. Embo Journal. 2001; 20:4214–21. [PubMed: 11483524]
51. McDaniel BA, Grundy FJ, Kurlekar VP, Tomsic J, Henkin TM. Identification of a mutation in the Bacillus subtilis S-adenosyhnethionine synthetase gene that results in derepression of S-Box gene expression. Journal of Bacteriology. 2006; 188:3674–81. [PubMed: 16672621]
52. Montange RK, Mondragon E, van Tyne D, Garst AD, Ceres P, Batey RT. Discrimination between Closely Related Cellular Metabolites by the SAM-I Riboswitch. Journal of Molecular Biology. 2010; 396:761–72. [PubMed: 20006621]
53. Stoddard CD, Montange RK, Hennelly SP, Rambo RP, Sanbonmatsu KY, Batey RT. Free state conformational sampling of the SAM-I riboswitch aptamer domain. Structure. 2010; 18:787–97. [PubMed: 20637415]
54. Stoddard CD, Widmann J, Trausch JJ, Marcano-Velazquez JG, Knight R, Batey RT. Nucleotides Adjacent to the Ligand-Binding Pocket are Linked to Activity Tuning in the Purine Riboswitch. Journal of Molecular Biology. 2013; 425:1596–611. [PubMed: 23485418]
55. Rode AB, Endoh T, Sugimoto N. Tuning Riboswitch-Mediated Gene Regulation by Rational Control of Aptamer Ligand Binding Properties. Angewandte Chemie-International Edition. 2015; 54:905–9.
56. Stelzer AC, Kratz JD, Zhang Q, Al-Hashimi HM. RNA Dynamics by Design: Biasing Ensembles Towards the Ligand-Bound State. Angewandte Chemie-International Edition. 2010; 49:5731–3.
57. Batey RT. Structure and mechanism of purine-binding riboswitches. Quarterly Reviews of Biophysics. 2012; 45:345–81. [PubMed: 22850604]
58. Montange RK, Batey RT. Riboswitches: Emerging themes in RNA structure and function. Annual Review of Biophysics. 2008:117–33.
59. Sambrook, J.; Russel, DW. Molecular Cloning: A laboratory manual. 3. Cold Spring Harbor, NY: Cold Spring Harbor Laboratory Press; 2001.
60. Trausch JJ, Ceres P, Reyes FE, Batey RT. The structure of a tetrahydrofolate-sensing riboswitch reveals two ligand binding sites in a single aptamer. Structure. 2011; 19:1413–23. [PubMed: 21906956]
61. Edwards AL, Batey RT. A Structural Basis for the Recognition of 2 '-Deoxyguanosine by the Purine Riboswitch. Journal of Molecular Biology. 2009; 385:938–48. [PubMed: 19007790]
62. Wilkinson KA, Merino EJ, Weeks KM. Selective 2 '-hydroxyl acylation analyzed by primer extension (SHAPE): quantitative RNA structure analysis at single nucleotide resolution. Nature Protocols. 2006; 1:1610–6. [PubMed: 17406453]
63. Das R, Laederach A, Pearlman SM, Herschlag D, Altman RB. SAFA: Semiautomated footprinting analysis software for high-throughput quantification of nucleic acid footprinting experiments. Rna-a Publication of the Rna Society. 2005; 11:344–54.
64. Waterhouse AM, Procter JB, Martin DMA, Clamp M, Barton GJ. Jalview Version 2-a multiple sequence alignment editor and analysis workbench. Bioinformatics. 2009; 25:1189–91. [PubMed: 19151095]
65. Griffiths-Jones S. RALEE-RNA ALignment Editor in Emacs. Bioinformatics. 2005; 21:257–9. [PubMed: 15377506]
66. Schroeder KT, McPhee SA, Ouellet J, Lilley DMJ. A structural database for k-turn motifs in RNA. Rna-a Publication of the Rna Society. 2010; 16:1463–8.

## Highlights

- Internal loop adjacent to the SAM recognition site is critical for binding
- Strong coupling between individual tertiary interactions of the PK1 subdomain
- Secondary structural element in P2 implicated in regulatory tuning
- Coupled network of interactions key for high fidelity co-transcription folding

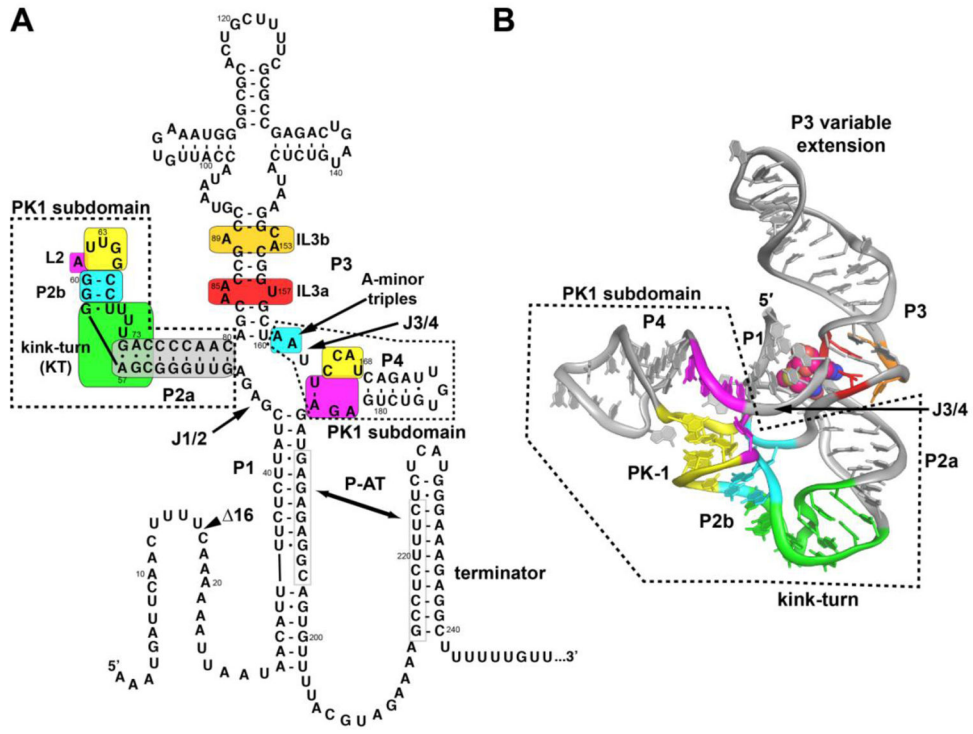


**Fig. 1.**

Secondary and tertiary structure of the SAM-I riboswitch. (A) Secondary structure of the *B. subtilis metE* SAM-I riboswitch based upon the crystal structures of the *T. tengcongensis metF-H2* and *B. subtilis yitJ* crystal structures. Colored boxes highlight regions of the RNA's structure that are the subject of this study. The PK1 subdomain (dashed box) encompasses the pseudoknot (residues 62–65 and 165–168; yellow), the kink-turn (residues 55–58 and 68–74; green), adenine-minor triples (residues 59, 60, 66, 67, 161, and 162; cyan) and a conserved base triple containing element (residues 61, 164, and 182–184; magenta). The P3 region encompasses part of the binding pocket within internal loop 3a (residues 84–85 and 157; red) as well as an additional internal loop 3b (residues 89 and 153–154; orange). B) The crystal structure of the *B. subtilis yitJ* SAM-I riboswitch aptamer domain (PDB 4KQY) to emphasize the three-dimensional relationship between the various conserved elements. The coloring scheme is the same as in (A).

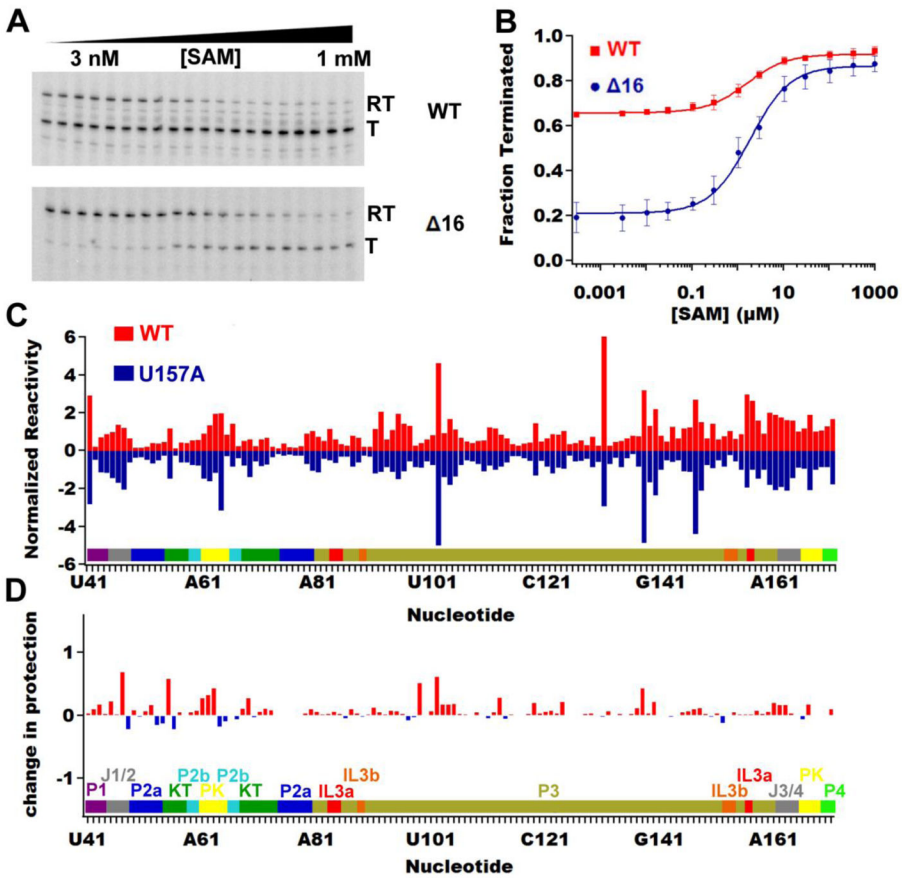


**Fig. 2.**

Validation of *metE* riboswitch function and structure. (A) Single-turnover *in vitro* transcription assays of the wild type *metE* riboswitch (top) and the Δ16 variant (bottom) as a function of SAM concentration. The bands corresponding to readthrough (RT) and terminated (T) transcription are denoted. (B) Quantification and analysis of the *in vitro* transcription assays for the wild-type (red squares) and the Δ16 variant (blue circles) of the *metE* riboswitch. Both RNAs have the same $T_{50}$ values but markedly different dynamic ranges because of the initial level of terminated product in the wild type riboswitch. (C) NMIA chemical probing (SHAPE) data showing that the aptamer domain from the U157A mutant (negative blue bars) has the same reactivity profile as the ligand free wild-type aptamer (positive red bars). Raw data in the form of the imaged sequencing gel is shown in Fig. S2 in the Supplementary Information. (D) Comparing the difference in SHAPE reactivity with and without ligand on the U157A mutant shows that SAM has no effect on the SHAPE reactivity of the U157A mutant.

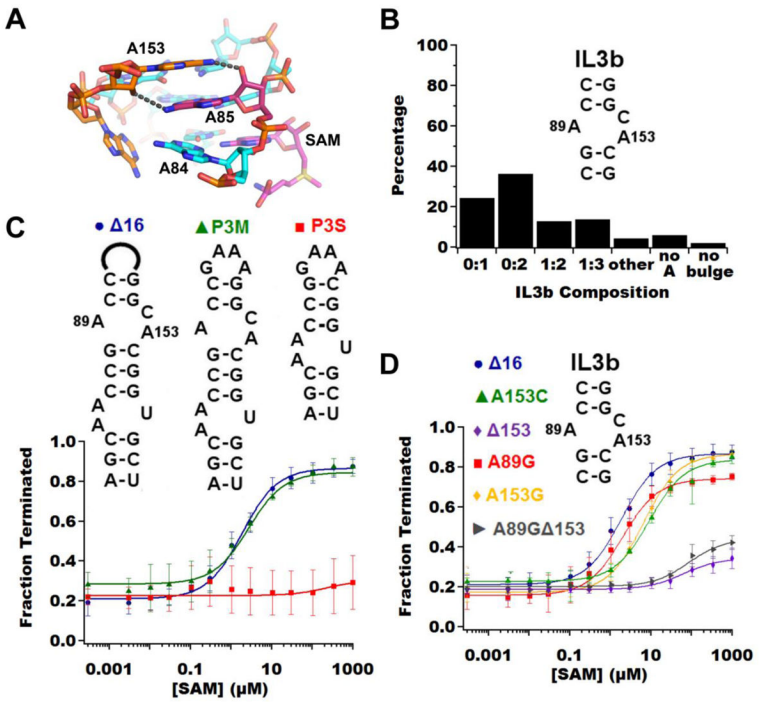


**Fig. 3.**

Analysis of the P3 helix of the *metE* riboswitch reveals the importance internal loop 3b (IL3b) has on stabilizing the binding pocket. (A) Closeup of the P3 helix from the *yitJ* (PDB:4KQY) crystal structure shows that adenine 85 in IL3a interacts with adenine 153 (numbering corresponds with the *B. subtilis metE* sequence) in the major groove of the RNA away from SAM. Dashed lines represent reciprocal hydrogen bonds between the base N6 and 2'-hydroxyl of the two adenosine residues. This perspective is a 180° rotation of the perspective shown in Figure 1B. (B) Bar graph representing the percentage of occurrence in our subset of SAM-I riboswitches for various bulge compositions for IL3b. The x-axis refers to the number of unpaired nucleotides defining the internal loop (5'-side:3'side); all loops considered in the 0:1, 0:2, 1:2, 1:3 and other have an unpaired adenine at the 3'-end of the 3'-side of the internal loop that would correspond to A153 in *metE*. (C) Quantified *in vitro* transcription assay of three P3 length variants (top) demonstrating that only when IL3b is removed (P3S, red squares) is the transcription termination efficiency affected. (D) Quantified *in vitro* transcription assay of IL3b mutations showing that the major contributing factor to the decrease in riboswitch function within IL3b is adenine 153.

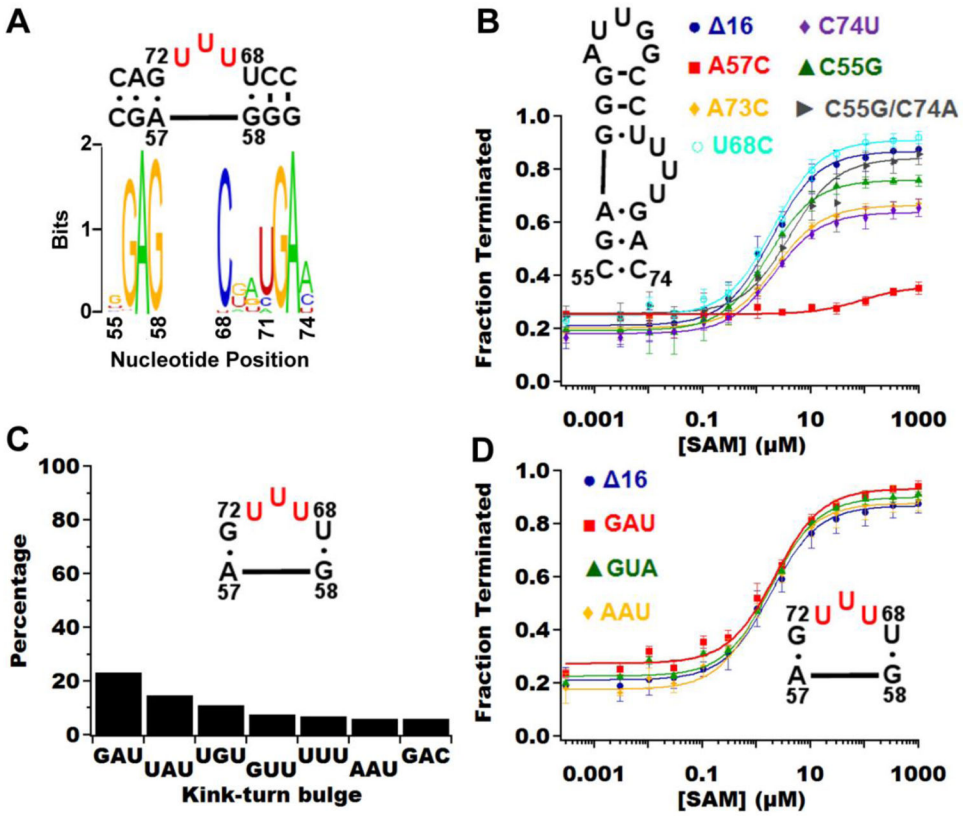


**Fig. 4.**

Analysis of the kink-turn in the *metE* riboswitch. (A) Shannon entropy plot of kink-turn sequences from the bioinformatics subset shows the sequence variation within the bulge region (residues 69–71) and at residues 55 and 74. Note that *metE* diverges from the phylogenetic consensus at positions 55, 68 and 74, which are cytosine, uracil and cytosine in *metE*, respectively. The general consensus kink-turn motif over all biological representatives is the two G•A pairs corresponding to G56•A73 and A57•G72 with all other positions being nucleotides that preserve the pattern of pairing [66]. (B) Quantified *in vitro* transcription assay of the kink-turn mutations reveals that only adenine 57 (red squares) is critical for maintaining the kink-turn in the context of the whole riboswitch. (C) Bar graph representing the percentage of occurrence in our subset of SAM-I riboswitches for the top seven bulge compositions. All other bulge compositions show up less than 3% of the time. (D) Graph of the *in vitro* transcription assay on the kink-turn bulge demonstrating that the riboswitch is highly tolerant of sequence variation at this site.

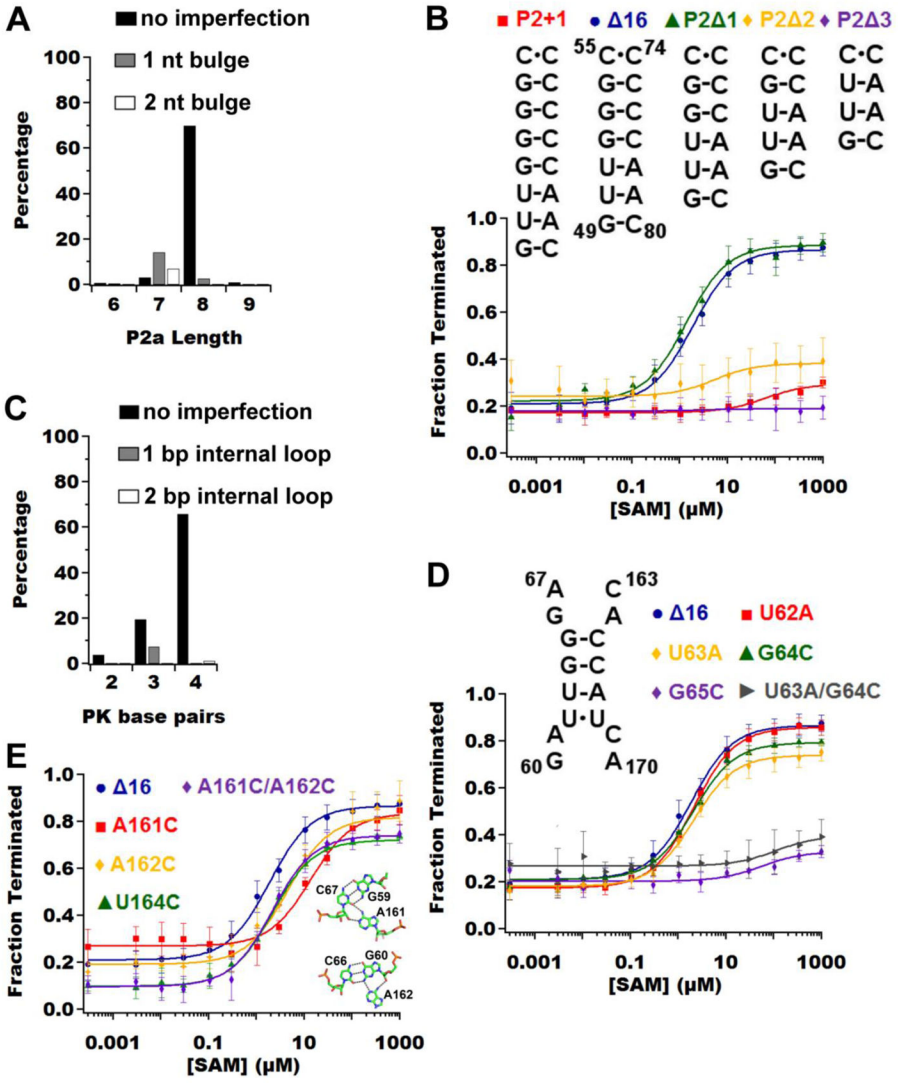


**Figure 5.**

Analysis of the pseudoknot in the *metE* riboswitch. (A) Bar graph representing the percentage of occurrence in our subset of SAM-I riboswitches for various lengths of P2a with different imperfections. P2a is defined as nucleotides 49 – 57 and 72 – 80, therefore in *metE* the length of P2a is nine base-pairs. (B) Quantificatied *in vitro* transcription assays of P2a length variants reveals P2a lengths of eight and nine base-pairs are tolerated. (C) Bar graph representing the percentage of occurrence in our subset of SAM-I riboswitches for various number of base pairs in the pseudoknot with different imperfections. (D) Quantificatied *in vitro* transcription assays of the base pairs variation in the pseudoknot reveals reveal that only the single point mutation of guanosine 65 (purple diamonds) causes the riboswitch to perform poorly. A double mutation (U63A/G64C, gray triangles), which results in only one base pair for the pseudoknot also causes the riboswitch not to function. (E) Quantificatied*in vitro* transcription assays of the adenine-minor triples reveals that the base triple directly adjacent to the pseudoknot (A161C, red squares) is most critical. The inset shows the two sets of base triples between P2b and J3/4.

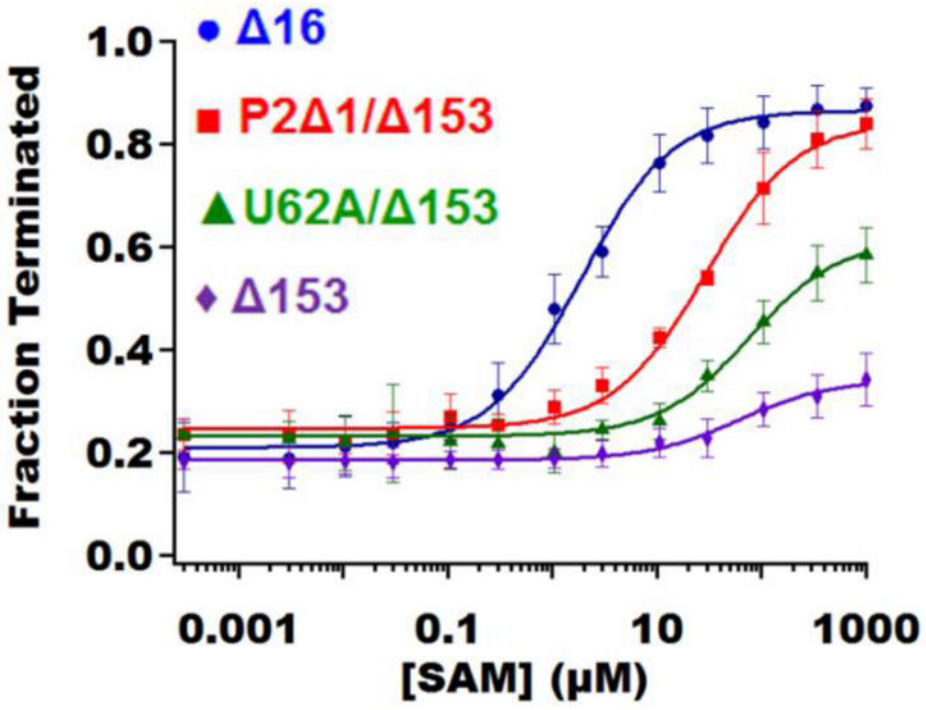


**Fig. 6.**

Analysis of double mutants of *metE* reveals that the loss in function by the deletion of adenine 153 (purple diamonds) can be partially restored by strengthening the pseudoknot (green triangles) or by repositioning of the terminal loop of P2, which forms the pseudoknot, through deletion of a base-pair in P2a (red squares). Quantification of the *in vitro* transcription assay of the wild type sequence (Δ16, blue circles) is shown for comparison.

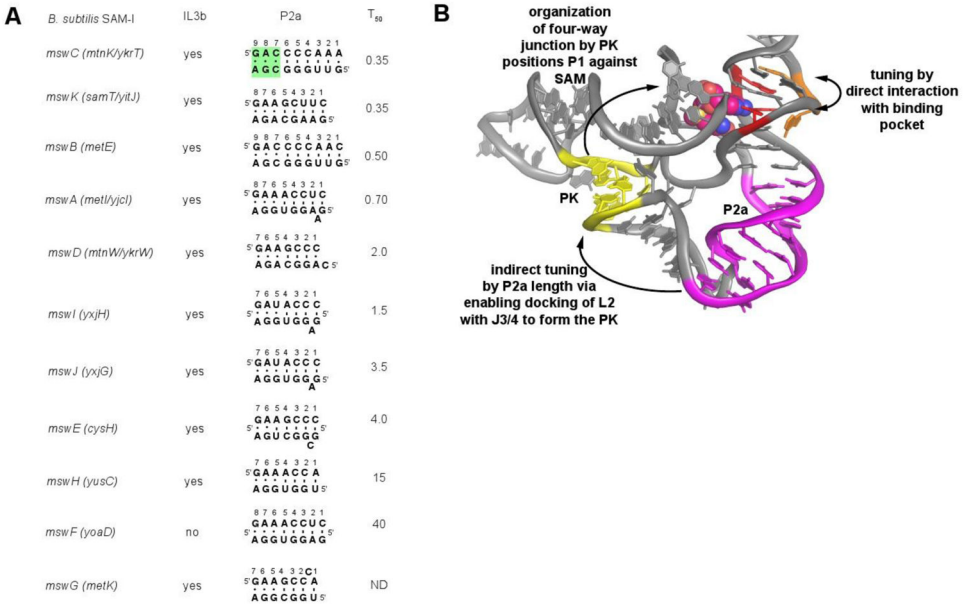


**Fig. 7.**

Model for regulatory tuning in *B. subtilis* SAM-I riboswitches. (A) Secondary structure of the P2a helix of the eleven SAM-I riboswitches. For each variant, the riboswitch gene names, presence of an internal loop 3b, secondary structure of the P2a helix and the observed $T_{50}$ value from the study by Tomsic *et al* [29] are given. The numbering of the P2a helix starts from the 5′-side of the helix, with the first nucleotide corresponding to the nucleotide following the universally conserved GA step in J1/2 (nt 47-48, Fig. 1) that is part of the SAM binding pocket. The last pair corresponds to the universally conserved A57-G72 pair of the kink-turn module; the green shading highlights the three noncanonical base pairs in P2a that are part of the kink-turn module. (B) Tertiary structure of the SAM-I riboswitch shows relationship of the two tuning element IL3b (orange) and P2a (magenta) relative to the SAM binding site (red) and SAM (van der Waals spheres). The pseudoknot that organizes the PK1 subdomain is shown in yellow.

**Table 1**

*In vitro* transcription mutational analysis of the *B. subtilis metE* SAM-I riboswitch

| Tertiary Element | Variant | $T_{50,obs}$, (μM) | Dynamic Range | Fraction terminated, (−) SAM | Fraction terminated, (+) SAM |
|---|---|---|---|---|---|
| | wild type | 1.6 ± 0.4 | 0.26 ± 0.01 | 0.66 ± 0.01 | 0.92 ± 0.01 |
| | Δ16 | 1.9 ± 0.5 | 0.66 ± 0.03 | 0.21 ± 0.02 | 0.87 ± 0.03 |
| IL3a | U157A | N.D. | N.D. | N.D. | N.D. |
| P3 | P3S | N.D. | N.D. | N.D. | N.D. |
| | P3M | 2.8 ± 0.6 | 0.56 ± 0.03 | 0.28 ± 0.03 | 0.84 ± 0.03 |
| IL3b | A89G | 2.0 ± 0.7 | 0.58 ± 0.03 | 0.16 ± 0.03 | 0.74 ± 0.03 |
| | A153C | 9 ± 1 | 0.61 ± 0.02 | 0.23 ± 0.01 | 0.84 ± 0.02 |
| | A153G | 6.6 ± 0.9 | 0.69 ± 0.02 | 0.17 ± 0.01 | 0.86 ± 0.02 |
| | Δ153 | 60 ± 60 | 0.16 ± 0.05 | 0.19 ± 0.01 | 0.35 ± 0.05 |
| | A89G/Δ153 | 90 ± 4 | 0.24 ± 0.04 | 0.20 ± 0.01 | 0.44 ± 0.04 |
| Kink-turn | A57C | 90 ± 70 | 0.10 ± 0.02 | 0.25 ±0.01 | 0.35 ± 0.02 |
| | A73C | 2.2 ± 0.4 | 0.46 ± 0.01 | 0.20 ± 0.01 | 0.66 ± 0.01 |
| | U68C | 2.1 ± 0.3 | 0.65 ± 0.01 | 0.24 ± 0.01 | 0.89 ± 0.01 |
| Kink-turn–bulge | GAU | 2.2 ± 0.3 | 0.66 ± 0.01 | 0.27 ± 0.01 | 0.93 ± 0.01 |
| | GUA | 1.9 ± 0.1 | 0.67 ± 0.01 | 0.22 ± 0.01 | 0.89 ± 0.01 |
| | AAU | 1.5 ± 0.2 | 0.70 ± 0.03 | 0.17 ± 0.01 | 0.87 ± 0.03 |
| Kink-turn 3b•3n | C55G | 1.7 ± 0.5 | 0.57 ± 0.02 | 0.19 ± 0.02 | 0.76 ± 0.02 |
| | C74G | 1.7 ± 0.7 | 0.53 ± 0.04 | 0.20 ± 0.03 | 0.73 ± 0.04 |
| | C74U | 2.1 ± 0.3 | 0.46 ±0.02 | 0.18 ± 0.01 | 0.64 ± 0.02 |
| | C55G/C74A | 4 ± 1 | 0.58 ± 0.03 | 0.26 ± 0.02 | 0.84 ± 0.03 |
| P2a length | P2+1bp | 60 ± 50 | 0.12 ± 0.02 | 0.17 ± 0.01 | 0.29 ± 0.02 |
| | P2Δ1bp | 1.4 ± 0.4 | 0.66 ± 0.03 | 0.22 ± 0.01 | 0.88 ± 0.03 |
| | P2Δ2bp | N.D. | N.D. | N.D. | N.D. |
| | P2Δ3bp | N.D. | N.D. | N.D. | N.D. |
| Pseudoknot–Composition | G64C/G65C | 70 ± 30 | 0.08 ± 0.01 | 0.23 ± 0.01 | 0.31 ± 0.01 |
| | U62A | 2.1 ± 0.3 | 0.68 ± 0.02 | 0.17 ± 0.01 | 0.85 ± 0.02 |

| Tertiary Element | Variant | $T_{50,obs}$, (μM) | Dynamic Range | Fraction terminated, (−) SAM | Fraction terminated, (+) SAM |
|---|---|---|---|---|---|
| | U62C/U168G | 1.8 ± 0.2 | 0.57 ± 0.01 | 0.23 ± 0.01 | 0.80 ± 0.01 |
| | U63A | 2.1 ± 0.2 | 0.58 ± 0.01 | 0.21 ± 0.01 | 0.79 ± 0.01 |
| | G64C | 2.1 ± 0.4 | 0.56 ± 0.02 | 0.18 ± 0.01 | 0.74 ± 0.02 |
| | G65C | 60 ± 30 | 0.13 ± 0.02 | 0.20 ± 0.01 | 0.33 ± 0.02 |
| | U63A/G64C | 100 ± 300 | 0.13 ± 0.09 | 0.27 ± 0.02 | 0.40 ± 0.09 |
| Pseudoknot–base triples | A61C | 2.7 ± 0.3 | 0.56 ± 0.01 | 0.20 ± 0.01 | 0.76 ± 0.01 |
| | U164C | 2.2 ± 0.3 | 0.62 ± 0.01 | 0.10 ± 0.01 | 0.72 ± 0.01 |
| | A161C | 14 ± 3 | 0.57 ± 0.03 | 0.27 ± 0.02 | 0.84 ± 0.03 |
| | A162C | 4.5 ± 0.9 | 0.63 ± 0.03 | 0.19 ± 0.01 | 0.82 ± 0.03 |
| | A161C/A162C | 2.2 ± 0.4 | 0.64 ± 0.03 | 0.10 ± 0.02 | 0.74 ± 0.03 |
| Double Mutants | Δ153 U62A | 80 ± 30 | 0.38 ± 0.05 | 0.23 ± 0.01 | 0.61 ± 0.05 |
| | Δ153 P2Δ1bp | 29 ± 5 | 0.60 ± 0.04 | 0.25 ± 0.01 | 0.85 ± 0.04 |

N.D. = not detected

**Table 2**

Isothermal Titration Calorimetry mutational analysis of the *B. subtilis metE* SAM-I riboswitch

| Construct | $K_{D, obs}$ (μM) | n |
|---|---|---|
| *B. subtilis metE* wild type | 0.079 ± 0.008 | 0.7 ± 0.2 |
| U157A | 24 ± 7 | 1.56 ± 0.02 |
| A89G/Δ153 | 16 ± 1 | 1.4 ± 0.2 |
| Δ153 | N.D. | N.D. |
| A89G | 0.09 ± 0.03 | 0.44 ± 0.04 |
| A153C | 0.15 ± 0.02 | 0.44 ± 0.04 |
| A153G | 0.15 ± 0.02 | 0.43 ± 0.03 |
| A57C | N.D. | N.D. |
| G64C/G65C | N.D. | N.D. |
| P2+1bp | N.D. | N.D. |
| P2Δ1bp | 0.046 ± 0.005 | 0.84 ± 0.03 |
| P2Δ2bp | 19 ± 4 | 0.50 ± 0.04 |
| *Tte metF-H2* WT | 0.07 ± 0.01 | 1.1 ± 0.1 |
| *Tte metF-H2* Δ60 | 0.6 ± 0.2 | 1.4 ± 0.2 |
| Δ153 U62A | 8 ± 2 | 2.0 ± 0.1 |
| Δ153 P2Δ1bp | 2.3 ± 0.5 | 1.1 ± 0.1 |

N.D. = not detected